Miniature End-Capped Fiber Sensor for Refractive Index and Temperature Measurement

Xuan-Yu Zhang, Yong-Sen Yu, Cong-Cong Zhu, Chao Chen, Rui Yang, Yang Xue, Qi-Dai Chen, and Hong-Bo Sun, *Member, IEEE*

***Abstract*— We have demonstrated an end-of-fiber polydimethylsiloxane (PDMS) cap based fiber Fabry–Pérot interferometer in this letter, which could be used for simultaneous measurement of refractive index (RI) and temperature with extremely low cross sensitivity. The RI and temperature sensitivities of the interferometer are −240.425 dB/RI unit based on extinction ratio measurement in the RI range of 1.3625–1.4150 and 385.46 pm/°C in the temperature range of 25 °C–60 °C, respectively. Not only does the interferometer have the characteristics of high sensitivity and low cost, but also PDMS has a good biocompatibility, so that the sensor can be used as a cell culture or bacteria growth detection probe.**

***Index Terms*— Fabry–Pérot interferometer (FPI), fiber sensor, multi-parameter sensing, polydimethylsiloxane (PDMS).**

I. Introduction

IN THE past few decades, fiber Fabry–Pérot interferometers (FFPIs) have been extensively studied, because they have the advantages of immunity to electromagnetic radiation, high sensitivity, corrosion resistance and low cost. They have been widely used to detect the physical and biochemical parameters. Several techniques have been developed to fabricate FFPIs with good characteristics and smart structures, such as laser microfabrication [1], fusion splicing [2]–[3] and chemical etching [4]. Nevertheless, they usually need a costly laser system or special fibers, such as photonic crystal fibers or doped fibers, which increase the cost and complexity of the fabrication process [1]–[4]. Meanwhile, FFPIs made of all-silica structure may limit their sensitivities. A way avoiding these problems by simply creating a polymer cap at the end face of the fiber has attracted lots of attention recently, such as the electrostatic self-assembly [5], spin-coating [6], self-guiding photopolymerization [7] and dip-coating methods [8]–[10]. The dip-coating method is a prior one that benefits from forming high quality reflection face and the high fabrication efficiency. However, the sensors fabricated with these methods are confined to single parameter measurement due to the structure and material, such as pH [5], refractive index (RI) [6]–[7], temperature [8] measurement and biochemical detection [9]–[10]. How to distinguish the measurands simultaneously with high sensitivity when several perturbations are applied is more important in practical applications. Especially, the simultaneous RI and temperature measurement, which are the basic parameters of the physical and biochemical systems. Unfortunately, it is not easy due to the cross sensitivity among measurands [11]–[12].

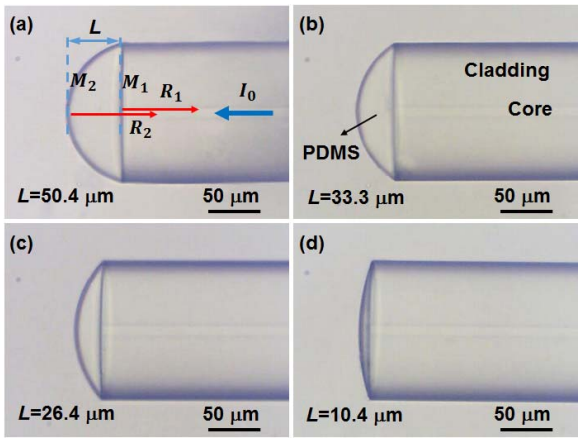

Fig. 1. (a)-(d) The microscope images of the EFFPI with different cavity length. The operation principle of the interference at the fiber tip is illustrated in (a).

In this letter, we have proposed and demonstrated a compact end-capped fiber Fabry–Pérot interferometer (EFFPI) by the dip-coating method, which can be used for simultaneous measurement of surrounding RI (SRI) and temperature with extremely low cross sensitivity. The operation principle of the sensor is based on the two beam interference of the reflection from the end face of fiber and polydimethylsiloxane (PDMS). We have exploited the advantages of PDMS: hydrophobicity, good transparency, nontoxicity and ease of synthesis. The EFFPI has a high sensitivity based on extinction ratio (ER) and wavelength shift measurement for SRI and temperature, respectively. We have also discussed the unique response of the EFFPI on ER with SRI change that has not been reported before.

II. Experiments and Theoretical Model

The structures of the sensors with different cavity length are illustrated in Fig. 1. The PDMS solution (Sylgard 184, Dow corning) used here was fully stirred with 10:1 mix ratio of base and curing agent and was centrifuged to exclude the air bubbles. Later, two sections of single mode fiber (SMF) (SMF-28e, Corning) with end-tip cleaved were clamped by the fusion splicer (FSU-975, Ericsson), one of which, marked as F_1, had a droplet of PDMS at the fiber end face by dipping

Manuscript received September 4, 2013; revised October 3, 2013; accepted October 11, 2013. Date of publication October 17, 2013; date of current version December 6, 2013. This work was supported by the National Natural Science Foundation of China under Grants 90923037, 91123027, and 61137001.

The authors are with the State Key Laboratory on Integrated Optoelectronics, College of Electronic Science and Engineering, Jilin University, Changchun 130012, China (e-mail: yuys@jlu.edu.cn; hbsun@jlu.edu.cn).

Color versions of one or more of the figures in this letter are available online at http://ieeexplore.ieee.org.

Digital Object Identifier 10.1109/LPT.2013.2286260

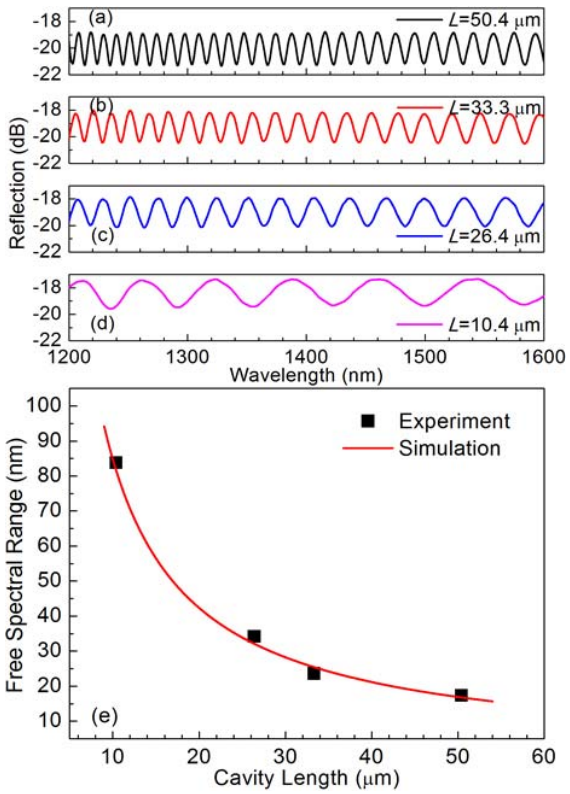

Fig. 2. (a)-(d) The reflection spectra of the EFFPI with different cavity length in air at 25 °C. (e) The FSR of the EFFPI as a function of cavity length at 1550 nm.

into the PDMS solution and the other one, marked as F_2, was connected to a supercontinuum broadband source (BBS) (Superk Compact, NKT Photonics) and an optical spectrum analyzer (OSA) (AQ6370, Yokogawa) via the 3 dB coupler. We contacted the end faces of the two fibers together with the help of the stepping motor of the fusion splicer. Then a smooth PDMS surface was formed at the end face of F_2 because of surface tension effect. The reflection spectrum of the EFFPI during the fabrication process was monitored by the OSA that has an amplitude resolution of 0.001 dB and a wavelength resolution of 0.02 nm. Increasing the contacting times, the PDMS left on F_1 would be decreased, therefore the PDMS dipped on F_2 also decreased and in this way the EFFPI with different cavity length could be fabricated. Afterwards, the fabricated EFFPI was vertically placed in an oven with the temperature of 105 °C for 2 hours to solidify the PDMS [13]. The reflection spectra of the EFFPI with different cavity length are shown in Figs. 2(a)-(d), from the spectra we can see that the longer cavity length corresponds to the larger loss, this may because of the longer cavity length, the light suffers more diffraction and scattering. The interference spectra are not very homogeneous, some high order guiding modes may be excited and join the interference that will affect the sensitivity of EFFPI. Fig. 2(e) shows the free spectral range (FSR) as a function of cavity length that is measured with a microscope.

The EFFPI proposed here can be described with the two beam interference theory based on Fresnel reflections, as shown in Fig. 1(a), I_0 is the incident light intensity. The EFFPI forms the first reflection surface M_1 at the interface of the SMF and the PDMS microsphere, the reflectivity of it comes to be $R_1 = \left|(n_{core} - n_{pdms})/(n_{core} + n_{pdms})\right|^2$, where n_{core} and n_{pdms} are the refractive indices of the core of the fiber and PDMS, respectively. The second reflection surface M_2 is formed between the PDMS microsphere and the surrounding medium. The second reflection surface can be regarded as a flat surface to the reflection, because the diameter of incident light point on F_2 equals to 18.2 μm that is small compared to the diameter of the cladding (numerical aperture of 0.14, cavity length of 50.4 μm) as discussed in [9]. The reflectivity of M_2 equals to $R_2 = \left|(n_{pdms} - n_{sur})/(n_{pdms} + n_{sur})\right|^2$, where n_{sur} is the refractive index of the surrounding medium.

According to [1], the normalized reflection spectrum of the interference can be expressed as:

$$R_{FP}(\lambda) = R_1 + M^2 R_2 + 2\sqrt{M^2 R_1 R_2} \times \cos(4\pi n_{pdms} L/\lambda + \delta(\pi)) \quad (1)$$

Where, the loss item $M = (1-\alpha)(1-A_1)$, α is the loss factor of the PDMS cavity, A_1 is transmission loss factor of the first reflection surface. L is the cavity length, λ is the wavelength of the incident light and $\delta(\pi)$ means there exists a π phase shift when $n_{sur} > n_{pdms}$ [1].

From Eq. (1), the ER can be expressed as:

$$\eta_{ER} = 10\log_{10}\left(\frac{R_1 + M^2 R_2 + 2\sqrt{M^2 R_1 R_2}}{R_1 + M^2 R_2 - 2\sqrt{M^2 R_1 R_2}}\right). \quad (2)$$

III. Sensing Characteristics and Discussion

Here, the EFFPI used for measurement of SRI and temperature has a cavity length of 50.4 μm as illustrated in Fig. 1(a), and the EFFPI was dipped in the sodium bromide solutions of different concentrations that had a RI range of 1.3317 $\sim$ 1.4236 calibrated by the Abbe refractometer to measure the SRI response and ultrasensitive fiber sensors based on wavelength [14] and peak loss [15] measurement have been reported before. We got a high sensitivity of -240.425 dB/RI unit (RIU) through the linear fitting of the experiment results in the RI range of 1.3625 $\sim$ 1.4150, which is the highest based on ER measurement of FFPIs [1]–[3], [6], to our best knowledge. Then we use 3σ [16] to evaluate the sensor's resolution, which sums the standard deviations of the measured amplitude and the amplitude resolution of the OSA, the $3\sigma_{ER-RI}$ for ER based RI measurement comes to be 0.127 dB, then the resolution of the EFFPI for SRI sensing based on ER equals to 5.29×10^{-4} RIU.

From Fig. 3 we can see that the EFFPI has two inflection points when changing the SRI based on ER measurement, which is different from the FFPIs before [1]–[3]. Although the two beam interference theory has been well known, the first inflection point has never been explained and unfolded, which could help us to design a sensor required.

From Eq. (2), we can get the derivative of η_{ER} with respect to n_{sur}:

$$\dot{\eta}_{ER} = \frac{-80M\sqrt{R_1}n_{pdms}(n_{pdms} - n_{sur})}{\ln 10(R_1 - M^2 R_2)\sqrt{R_2}(n_{pdms} + n_{sur})^3} \quad (3)$$

The two inflection points can be explained by the monotonicity of η_{ER} in Eq. (3) based on the plus or minus

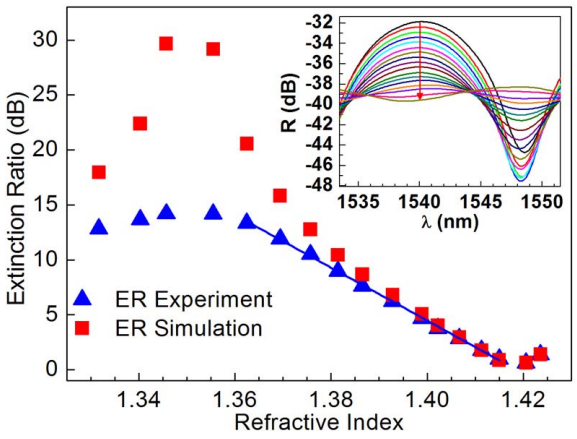

Fig. 3. The ER of the EFFPI changes with SRI, the blue solid line is the linear fitting of the experiment results in the RI range of 1.3625∼1.4150 around 1550 nm. Inset: reflection spectra monitored with different SRI and the red arrow represents the increase of the SRI.

sign of the value of $n_{pdms} - n_{sur}$ and $R_1 - M^2 R_2$. There exists a non-differentiable point that is the first inflection point when $R_1 = M^2 R_2$, this means we can get an infinite value based on ER measurement in theory, however, this is impossible in practice because the signal is too weak and can't be detected. When $n_{pdms} = n_{sur}$ we get the second inflection point, and R_2 gets the minimum value zero as well as η_{ER}. In the simulation, we adopt the following parameters: $\alpha = 0.02$, $A_1 = 0.4$, $n_{core} = 1.4592$, $n_{pdms} = 1.418$.

According to the calculation, when $R_1 = M^2 R_2$, n_{sur} equals to 1.351 or 1.489. So in the RI range of 1.3317∼ 1.4206, $n_{sur} = 1.351$ will be the first inflection point. And $n_{sur} = 1.418$ will be the second inflection point because the Fresnel reflection of the second interface equals to zero. We find that in the RI range of 1.3317 ∼ 1.3757, the simulation and the experiment don't agree well because the power range exceeds the detection range of the OSA. The first inflection point may cause a problem when demodulate the signal, however, the analysis above can help us to design a sensor with the similar sensing mechanism to avoid it. To achieve this, the RI of the material coated on the fiber end-tip should be smaller than 1.411 or larger than 1.661. And we can achieve a higher sensitivity with an OSA with a higher detection range, as shown in Fig. 3, the simulation curve has a bigger slope than the experiment curve. The second inflection point can be demodulated with the π phase shift.

Afterwards, we researched the response of the sensor to SRI based on normalized peak intensity (ΔP) measurement. And got a sensitivity of −79.17 dB/RIU in the RI range of 1.3317 ∼ 1.4150 that is about 4 times higher than [3] as shown in Fig. 4(a), from it we can see that the experiment and the simulation agree well. According to the calcultion, the $3\sigma_{NPI-RI}$ for ΔP based RI measurement comes to be 0.0728 dB, then the resolution of the EFFPI fabricated for SRI based on ΔP equals to 9.2×10^{-4} RIU. The SRI sensitivity based on wavelength shift ($\Delta\lambda$) measurement is 0.08927 nm/RIU. Then the EFFPI sensor was sealed in a small long tube that was dipped in the oil bath tank with

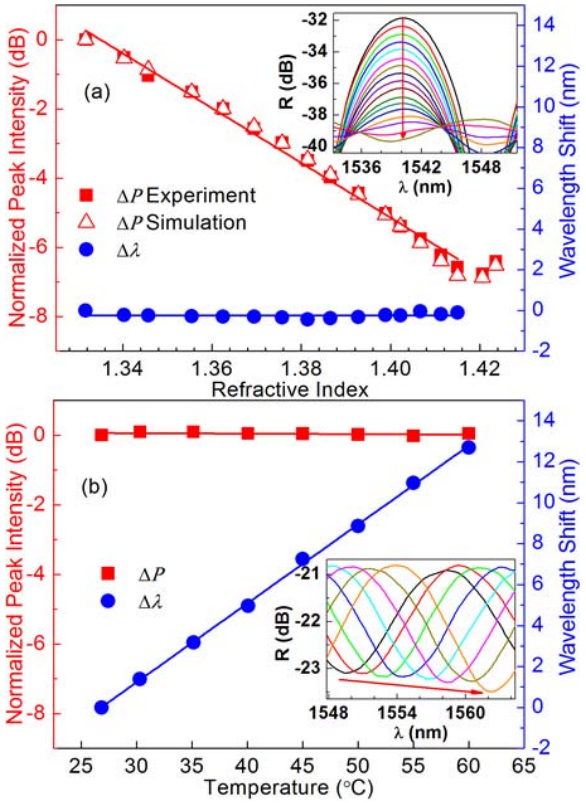

Fig. 4. (a) ΔP and $\Delta\lambda$ change with SRI around 1550 nm, the solid red line and blue line are the linear fitting of ΔP experiment and $\Delta\lambda$, respectively. (b) ΔP and $\Delta\lambda$ change with temperature. Insets: reflection spectra monitored when changing SRI and temperature, and the red arrow represents the increase of SRI and temperature, respectively.

a resolution of 0.01 °C to conduct the temperature sensing. We got a sensitivity of 385.46 pm/°C in the temperature range of 25 °C∼ 60 °C based on $\Delta\lambda$ measurement, which is about 30 times higher than the FFPIs with all-silica structures [11], [17], and [18] and higher than most FFPIs had reported until now. According to the standard deviations of measured wavelength and wavelength resolution of the OSA, $3\sigma_{WL-TEM}$ for wavelength based temperature measurement equals to 0.211nm, then the resolution to temperature of the sensor is 0.55 °C. The temperature sensitivity based on ΔP measurement is −0.00127 dB/°C. Therefore, the SRI and temperature cross sensitivities are extremely low, which are 0.2316 °C/RIU and 1.604×10^{-5} RIU/°C, respectively. To achieve a larger linear range for SRI measurement, we use the ΔP and $\Delta\lambda$ measurement for multi-parameter sensing. Then we get the SRI and temperature dual-parameter sensing matrix [17]:

$$\begin{pmatrix} \Delta P \\ \Delta\lambda \end{pmatrix} = \begin{pmatrix} \kappa_{P,n} & \kappa_{P,T} \\ \kappa_{\lambda,n} & \kappa_{\lambda,T} \end{pmatrix} \begin{pmatrix} \Delta n \\ \Delta T \end{pmatrix} = K \begin{pmatrix} \Delta n \\ \Delta T \end{pmatrix} \quad (4)$$

Where, Δn, ΔT represent the change of SRI and temperature. $\kappa_{P,n}$ and $\kappa_{\lambda,n}$ are the SRI sensitivities based on ΔP and $\Delta\lambda$ measurement. $\kappa_{P,T}$ and $\kappa_{\lambda,T}$ are the temperature sensitivities based on ΔP and $\Delta\lambda$ measurement. Substituting the sensitivities from the experiment into Eq. (4), we can get the sensing

matrix as follows:

$$\begin{pmatrix} \Delta n \\ \Delta T \end{pmatrix} = K^{-1} \begin{pmatrix} \Delta P \\ \Delta \lambda \end{pmatrix} = \frac{1}{|K|} \times \begin{pmatrix} 385.46 & 0.00127 \\ -89.27 & -79.17 \end{pmatrix} \begin{pmatrix} \Delta P \\ \Delta \lambda \end{pmatrix} \quad (5)$$

The low $1/|K|$ (-3.28×10^{-5}) that quantifies the discrimination between SRI and temperature [19] represents the good discrimination between SRI and temperature of the EFFPI. Then we use the condition number of the matrix to assess the performance of the EFFPI, which provides an indication of the sensitivity of the matrix operation to uncertainties in the matrix elements [20]. This matrix is reasonably well conditioned, having a very low condition number of $cond(K) = 5.14$ that is far less than [11]–[12], hence inverting it permits the recovery of SRI and temperature measurements from the response data.

IV. Conclusion

In conclusion, we have demonstrated a compact EFFPI with a PDMS cap at the end of the SMF, which was fabricated by the dipping method. The EFFPI has a high sensitivity to SRI based on ER measurement, which is -240.425 dB/RIU in the range of $1.3625 \sim 1.4150$ and we also analyzed the response of the sensor to SRI that could be used to design a sensor with the similar sensing mechanism. As for ΔP based measurement for SRI, the sensitivity is -79.17 dB/RIU, and the sensitivity for temperature is 385.46 pm/°C that is about 30 times larger than the FFPIs with all-silica structures. The sensor has an extremely low cross sensitivity, and the dual-parameter sensing characteristic of the sensor for SRI and temperature is discussed as well. The biocompatibility, compact structure, high sensitivity strong points of the sensor make it a prior choice for biochemical and fixed point sensing.

References

[1] Z. L. Ran, Y. J. Rao, W. J. Liu, X. Liao, and K. S. Chiang, "Laser-micromachined Fabry-Perot optical fiber tip sensor for high-resolution temperature independent measurement of refractive index," *Opt. Express*, vol. 16, no. 3, pp. 2252–2263, Feb. 2008.

[2] B. Dong, J. Z. Hao, T. S. Zhang, and J. L. Lim, "High sensitive fiber-optic liquid refractive index tip sensor based on a simple inline hollow glass micro-sphere," *Sens. Actuators B, Chem.*, vol. 171, pp. 405–408, Aug. 2012.

[3] C. L. Lee, M. Li, J. M. Hsu, J. S. Horng, W. Y. Sung, and C. M. Li, "Microcavity fiber Fabry-Pérot interferometer with an embedded golden thin film," *IEEE Photon. Technol. Lett.*, vol. 25, no. 9, pp. 833–836, May 15, 2011.

[4] Y. Gong, Y. J. Rao, Y. Guo, Z. L. Ran, and Y. Wu, "Temperature-insensitive micro Fabry-Pérot strain sensor fabricated by chemically etching Er-doped fiber," *IEEE Photon. Technol. Lett.*, vol. 21, no. 22, pp. 1725–1727, Nov. 15, 2009.

[5] J. Goicoechea, C. R. Zamarreño, I. R. Matias, and F. J. Arregui, "Utilization of white light interferometry in pH sensing applications by mean of the fabrication of nanostructured cavities," *Sens. Actuators B, Chem.*, vol. 138, no. 2, pp. 613–618, May 2009.

[6] J. R. Zhao, X. G. Huang, W. X. He, and J. H. Chen, "High-resolution and temperature-insensitive fiber optic refractive index sensor based on Fresnel reflection modulated by Fabry-Perot interference," *J. Lightw. Technol.*, vol. 28, no. 19, pp. 2799–2803, Oct. 1, 2010.

[7] O. Frazão, *et al.*, "Fabry-Perot refractometer based on an end-of-fiber polymer tip," *Opt. Lett.*, vol. 34, no. 16, pp. 2474–2476, Aug. 2009.

[8] Q. Z. Rong, H. Sun, X. G. Qiao, J. Zhang, M. L. Hu, and Z. Y. Feng, "A miniature fiber-optic temperature sensor based on a Fabry-Perot interferometer," *J. Opt.*, vol. 34, no. 4, pp. 045002-1–045002-6, Apr. 2012.

[9] Y. T. Tseng, Y. J. Chuang, Y. C. Wu, C. S. Yang, M. C. Wang, and F. G. Tseng, "A gold-nanoparticle-enhanced immune sensor based on fiber optic interferometry," *Nanotechnology*, vol. 19, no. 34, pp. 345501-1–345501-5, Aug. 2008.

[10] R. B. Queirós, *et al.*, "Microcystin-LR detection in water by the Fabry-Pérot interferometer using an optical fibre coated with a sol-gel imprinted sensing membrane," *Biosens. Bioelectron.*, vol. 26, no. 9, pp. 3932–3937, May. 2011.

[11] R. Yang, Y. S. Yu, C. Chen, Q. D. Chen, and H. B. Sun, "Rapid fabrication of microhole array structured optical fibers," *Opt. Lett.*, vol. 36, no. 19, pp. 3879–3881, Oct. 2011.

[12] D. J. J. Hu, *et al.*, "Long period grating cascaded to photonic crystal fiber modal interferometer for simultaneous measurement of temperature and refractive index," *Opt. Lett.*, vol. 37, no. 12, pp. 2283–2285, Jun. 2012.

[13] A. C. Urness, E. D. Moore, K. K. Kamysiak, M. C. Cole, and R. R. McLeod, "Liquid deposition photolithography for submicrometer resolution three-dimensional index structuring with large throughput," *Light: Sci. Appl.*, vol. 2, pp. 56–58, Mar. 2013.

[14] S. C. Gao, *et al.*, "Ultrasensitive refractive index sensor based on micro-ber-assisted U-shape cavity," *IEEE Photon. Technol. Lett.*, vol. 25, no. 18, pp. 1815–1818, Sep. 1, 2013.

[15] J. C. Guo, *et al.*, "Compact long-period fiber gratings based on periodic microchannels," *IEEE Photon. Technol. Lett.*, vol. 25, no. 2, pp. 111–114, Jan. 15, 2013.

[16] I. M. White and X. D. Fan, "On the performance quantification of resonant refractive index sensors," *Opt. Express*, vol. 16, no. 2, pp. 1020–1028, Jan. 2008.

[17] C. Chen, *et al.*, "Compact fiber tip modal interferometer for high-temperature and transverse load measurements," *Opt. Lett.*, vol. 38, no. 17, pp. 3202–3204, Sep. 2013.

[18] C. Chen, *et al.*, "Reflective optical fiber sensors based on tilted fiber Bragg gratings fabricated with femtosecond laser," *J. Lightw. Technol.*, vol. 31, no. 3, pp. 455–460, Feb. 1, 2013.

[19] A. A. Clifford, *Multivariate Error Analysis: A Handbook of Error Propagation and Calculation in Many-Parameter Systems*. London, U.K.: Appl. Sci. Publishers, 1973.

[20] A. M. Vengsarkar, W. C. Michie, L. Jankovic, B. Culshaw, and R. O. Claus, "Fiber-optic dual-technique sensor for simultaneous measurement of strain and temperature," *J. Lightw. Technol.*, vol. 12, no. 1, pp. 170–177, Jan. 1994.